JOURNAL OF MATERIALS SCIENCE 33 (1998) 1451–1460

The effects of ageing condition on shear localization from the tip of a notch in maraging steel

J. J. MASON, J. A. ZIMMERMAN, K. M. ROESSIG
University of Notre Dame, Department of Aerospace and Mechanical Engineering, 365 Fitzpatrick Hall, Notre Dame, IN 46556-5637 USA

An experimental investigation of shear localization at the tip of a notch in several material states of 300 maraging steel is reported. Side-impacted edge-notched plates were tested in the under-aged, peak-aged, and over-aged conditions, and the critical impact velocity above which shear localization occurs at the notch tip is reported for a notch root radius of 175 μm. It is found that the critical minimum impact velocity required for shear localization is independent of the ageing condition. Next, the propagation of shear localization in two of the three ageing conditions is recorded using high speed photography at framing rates of 480 000 frames per second. It is seen that, within the uncertainty of the experimental method, shear localization initiates at approximately the same time and stress intensity factor for the two materials. A heavy dependence of the shear band propagation speed and final length upon the ageing condition is seen. For the conditions examined shear failure is seen to propagate at an average velocity of 1000 m s^{-1} in peak-aged material and 300 m s^{-1} in under-aged material. The peak-aged material fails fully by shear while the shear failure in under-aged material arrests and is followed by tensile failure. This result demonstrates the effect of material strength, roughly independent of the strain hardening characteristics for these materials, on shear localization propagation. The effects of the specimen and projectile geometry on the results are examined qualitatively using elastodynamic finite element analysis of the stationary notch tip loading.

1. Introduction

Metal failure by adiabatic shear localization has received increased attention in the last decade. Experimental results for several loading geometries, including the torsional split Hopkinson bar (TSHB) [1–3], punch tests [4] and notch tests [5–7], have been reported, and, as expected, many numerical simulations of the conditions which lead to the formation of adiabatic shear bands have also appeared. In most investigations only the initiation of adiabatic shear bands is considered where initiation is assumed to occur when thermal softening is greater than strain or strain-rate hardening. Zener and Holoman [8], in introducing this accepted explanation of shear localization initiation, postulated a criterion for shear localization that can be stated mathematically as [9]

$$\left(\frac{\partial\tau}{\partial\gamma}\right)+\left(\frac{\partial\tau}{\partial\dot{\gamma}}\right)\frac{d\dot{\gamma}/dt}{d\gamma/dt}+\left(\frac{\partial\tau}{\partial T}\right)\frac{\beta\tau}{\rho c_p}\leqslant 0 \qquad (1)$$

where τ is stress or material strength, γ is the plastic strain, $\dot{\gamma}$ is the strain rate, t is time, T is temperature, ρ is density, c_p is the heat capacity, and β is the fraction of plastic work converted to heat. This intuitive criterion has been mathematically verified using perturbation techniques on the equations describing the conservation of momentum and energy for situations in which strain rate is constant up to the point of localization [10]. In that case, it may be assumed that the second term in the above equation is negligible and the resulting criterion is [11]

$$\left(\frac{\partial\tau}{\partial\gamma}\right)+\left(\frac{\partial\tau}{\partial T}\right)\frac{\beta\tau}{\rho c_p}\leqslant 0 \qquad (2)$$

While the criterion in Equation 2 accurately describes the process of adiabatic shear band initiation, it does not give the engineer an easy criterion to implement nor lend itself to repeatable experiments with which to compare the shear localization susceptibility of various materials. In response, a critical strain criterion for shear localization has been suggested [11], and Batra and Kim [12], using empirical constitutive data in numerical simulations of TSHB tests, have been able to rank some materials' adiabatic shear susceptibility using that criterion. The critical strain in their numerical investigation is dependent upon the initial imperfection in the specimen, but the ranking did not change when the initial perfection was changed. This dependence of the localization on the initial imperfection led Chen and Batra [13] to examine the ranking of the same materials for the initiation

of a shear band at the tip of a crack or notch. In this case the critical strain criterion translates into a critical dynamic mode-II stress intensity factor, K^{d}_{IIc}, which depends upon dK^{d}_{IIc}/dt as well. Presumably, this critical dynamic mode-II stress intensity factor serves as a more robust measure of the susceptibility of the material with K^{d}_{IIc} ideally being a material parameter. This criterion shows promise for the experimentalist and materials scientist since it may be easier to reproducibly measure this critical stress intensity factor for various materials and because it relies on the more readily validated assumption that a singularity in the stress field exists and small scale yielding conditions prevail. However, the potential influence of more fundamental material parameters on K^{d}_{IIc} is not clear.

It is generally understood that microstructure does not play a dominant, primary role in shear localization [11]. However, Rogers [14], in summarizing much work on shear localization, has stated that a material's rate of strain hardening is the key factor in determining its susceptibility to shear localization; the implication being that a material's rate of strain hardening plays a dominant role in determining K^{d}_{IIc}. Thus, the effects of microstructure on the rate of strain hardening are important. However, glancing at the expression of the criterion in Equations 1 and 2, it is clear that the material strength, τ, plays a role as well. High strength leads to a larger heating term multiplying the thermal softening term, $\partial\tau/\partial T$, which can lead to a greater effective rate of thermal softening. The effect of strength is clouded, however, by the fact that, generally, strength and strain hardening rate are inversely related; the higher a material strength, the lower its strain hardening rate. So, in many cases, the effect of strain hardening rate indirectly demonstrates the effect of strength through the interdependence of these two characteristics. Through ageing treatments of maraging steel, we are, in this paper, able to demonstrate the effect of strength and rate of strain hardening roughly independent of each other.

Failure by adiabatic shear localization does not occur by initiation alone. It is a two-step process: initiation is followed by propagation. And while many investigations have looked at initiation of shear bands, surprisingly little study of the propagation of adiabatic shear bands has been performed [1, 3, 7, 15, 16]. Mason *et al.* [7] in a study of shear localization propagation from a notch tip in peak-aged 300 maraging steel report that shear localization immediately after initiation propagates at velocities of about $320\,m\,s^{-1}$. Zhou *et al.* [15] in their study of shear localization initiation from notch tips have reported that for the same steel shear band velocity depends upon the initial impact velocity and upon the extension length. Shear bands are seen to accelerate up to maximum speeds of $1000\,m\,s^{-1}$. During propagation Grady [17] has suggested that a fracture toughness approach might be used to characterize the energy dissipated in a propagating adiabatic shear band. And Zhou *et al.* [16], in a numerical study, have indicated that a relationship between the adiabatic shear localization velocity and the loading intensity or *J*-integral, similar to the relationship for dynamic mode-I crack propagation, may exist. The full nature of these relationships has yet to be explored for a variety of materials.

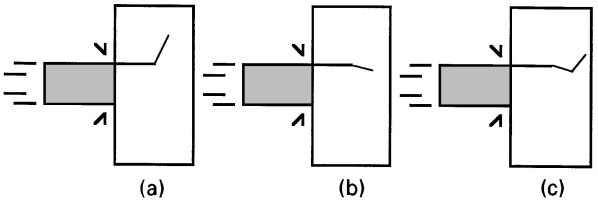

Figure 1 The geometry of the Kalthoff test. (a) Fracture path associated with crack opening mode seen by Kalthoff [5] at lower velocities. (b) Fracture due to shear seen by Kalthoff [5] at higher velocities. (c) Fracture seen by Mason *et al.* [7].

Experimentally, the Kalthoff geometry [5], shown schematically in Fig. 1, has proven useful in examining the relationship between the dynamic stress intensity factor at a notch or crack tip and the initiation and propagation of adiabatic shear bands there. Currently, however, only peak-aged 300 maraging steel and a titanium alloy have been tested in this geometry. Tests performed on 300 maraging steel show a shear localization or shear crack forming at the notch tip at early times after impact followed by propagation. In some cases, the shear failure arrests and a tensile crack is formed at a later time. Tests on titanium [16], which is often designated as one of the easiest materials to fail by shear localization [18], show that it is more resistant to shear band propagation in this geometry than 300 maraging steel. This might suggest that the geometry is not all that useful for testing shear localization, since full shear failure is difficult to attain with a material as easy to shear localize as titanium. Some further tests of the shear localization behaviour of 300 maraging steel in this geometry will be useful to make further assessment of the applicability of this technique to other, less shear band susceptible, materials.

In this work some results regarding shear localization and shear band propagation in Kalthoff tests on 300 maraging steel are reported. Variations on the experimental method of Kalthoff and coworkers [5, 6] and Rosakis and coworkers [7, 16] have been investigated with interest directed toward quantifying the effects of projectile length, the specimen size and the ageing condition of the material on the shear localization initiation and propagation behaviour. A high-speed photography system is used to take pictures of the specimen as it deforms shortly after impact; the transition from mostly shear to mostly tensile failure is recorded and velocities of the shear band are measured. Lastly, some simplistic finite element models are presented to explain the nature of the loading in the tests and to help interpret the experimental results.

2. Experimental method

Specimens were made of 300 maraging steel in three ageing conditions – under-aged, peak-aged, and over-aged – and machined into $50 \times 100 \times 6\,mm$ rectangles. A notch, 25 mm long and 37 mm from the top, as shown in Fig. 1, was machined through the thickness

using wire electron discharge machining (EDM) resulting in a notch tip radius of 175 μm. The specimen size was 1/2 that of Rosakis and coworkers [7, 16] and Kalthoff and coworkers [5, 6], leading to considerable cost savings on materials. The notch tip radius was not varied so that variations with respect to the material heat treatment and other experimental parameters could be studied independently; Kalthoff [5, 6] has characterized the effects of notch tip radius on the initiation and propagation of adiabatic shear bands in this geometry. The notch tip radius was also chosen to be small because for small radii the critical shear localization velocity has been shown to be low and relatively insensitive to variations in the radius [5, 6]. The specimens were impacted using an air gun and 50.8 mm and 152.4 mm long, 25.4 mm diameter projectiles made of 350 maraging steel in a peak-aged condition. The projectiles travelled with speeds up to $50\,\mathrm{m\,s^{-1}}$. Impact velocity is measured using an infrared detector–emitter pair mounted on the gun barrel. The influence of ageing condition, projectile length, and projectile velocity on the choice of failure mode was then observed.

Maraging 300 steel samples were solution-treated following guidelines from the ASM handbook [19], and then age-hardened for the following periods: 0.5, 1, 2, 4, 8, 16, 32, 64, and 128 h. Hardness tests using a Rockwell hardness tester were performed and under-aged, peak-aged, and over-aged conditions corresponding to 0.5, 4, and 124 h of heat treatment, respectively, were chosen. These three materials were then tested in tension following standard tension testing techniques.

Specimens from each ageing condition were impacted at a range of velocities until shear localization or any other type of fracture was observed. Failure was determined through observation of the fracture surface or by the presence of a visible crack. The effects of projectile length were examined by performing this sequence twice: once for the 50.8 mm projectile and once for the 152.4 mm projectile.

Two ageing conditions of the 300 maraging steel were impacted on the side with the 50 mm long projectile. High speed photographs were taken using a Cordin model 330 camera with a Cordin model 607 light source. A strain gauge was placed on the side of the plate near the impact area to record the elastic wave due to impact. This, in conjunction with a high speed light sensor used to detect the flash of the light source, gave the time of impact. Both the strain gauge signal and light sensor signal are recorded on a digital oscilloscope to give the timing, with respect to impact, of the recorded photographs. The location of the shear band tip is visible as a slight lightening of the material. This is caused by the formation of a very small dimple ahead of the shear band tip. Using the images, the location of the tip was recorded as a function of time. Some uncertainty was encountered in determining the location of the shear band tip because of the nature of the images, but by using high magnification comparisons of images in one frame to images in the previous and subsequent frames, the location of the shear band tip could be determined satisfactorily.

3. Numerical method

The finite element method was used to numerically examine the elastic wave propagation in the test specimens. This was necessary in order to properly interpret the results of the experiments. Lee and Freund [20] have provided the stress intensity history at the notch tip for short times after loading; here the behaviour for long times was investigated.

The finite element package ABAQUS/Standard [21] was used to perform the calculations. A uniform mesh of eight-noded, plane stress, square elements, 5×5 mm, was used to model the plate except in the area of the notch tip, where eight-noded quarter-point elements (QPEs) were concentrated to represent the notch tip as a crack tip. The stress intensity factor history was calculated using the William's expansion and the crack tip nodal displacements from the QPEs. This method has been show to be both efficient and simple in its application to transient dynamic analysis [22]. The time step was chosen following the recommendations of Murti and Valliappan [22] to reduce the amount of spurious oscillations in the results. The material in the model is linearly elastic with Poisson's ratio $\nu = 0.35$. It should be mentioned that plasticity was not modelled because the purpose was only to provide a means to qualitatively understand the experimental results. Fully thermoviscoplastic analysis of tests of this nature has been performed by Zhou *et al.* [15] and Batra and Nechitailo [23]. The models presented here are accurate indicators of the notch tip stress field, however, until conditions of small scale yielding are no longer valid. In some tests the assumption of small scale yielding may be valid for long times, in other tests it will only be valid before a shear band propagates a distance from the notch tip. In light of that caveat, several cases were examined.

First, the geometry of Mason *et al.* [24] was modelled to establish the validity of the method. As expected, good agreement was seen between the solution of Lee and Freund and the finite element solution for short times. Predicted stress intensity factors for long time also matched those measured experimentally quite well [25]. Long-time loading of the notch tip was seen to be dominated by stress wave reflections and reverberations in the specimen. Next, having verified the numerical method, the specimen used in these experiments was modelled when impacted by a rigid projectile and a 50 or 150 mm deformable projectile.

4. Results and discussion

The results of the numerical investigation are presented first so that they may be used in the discussion of the experimental investigation.

4.1. Numerical investigation of the effects of specimen and projectile size

The stress intensity factor history at the notch tip in side-notched, $50 \times 100 \times 6$ mm plates impacted from the side is shown in Fig. 2. The stress intensity factors are normalized by the same factor given by Lee and

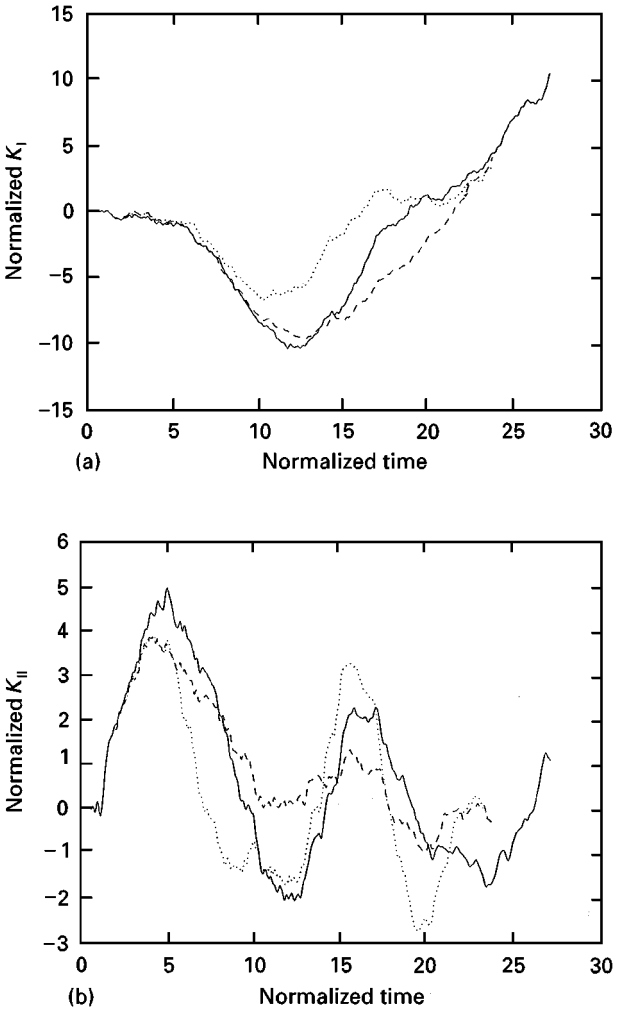

Figure 2 The dynamic (a) mode-I, K_I, and (b) mode-II, K_{II}, stress intensity factors for the current geometry with different projectile lengths. (—) Rigid projectile; (⋯) 50.8 mm; (- - -) 152.4 mm.

Freund [20]

$$K' = \left(\frac{l}{\pi}\right)^{1/2} \frac{Ev_0}{2c_d^{pl-\sigma}} \tag{3}$$

where E is Young's modulus, l is the crack length, v_0 is the velocity on the plate boundary, and $c_d^{pl-\sigma}$ is the plane stress dilatational wave speed. Time is normalized by the characteristic time, t', the time for a dilatational wave to reach the notch tip after impact, $t' = l/c_d$. For the steel tested here the normalized time is about 4.7 μs. Some similarities between the results for the deformable 50.8 and 152.4 mm projectiles and those for a rigid projectile can be seen. In Fig. 2b it is clear that K_{II} dominates the notch tip field until a normalized time of approximately 5, where it begins to decrease. The peak in K_{II} occurs at about the time the plane stress dilatational wave arrives at the crack tip for the second time (after being reflected from the back surface and then the impact surface). The rigid projectile has a larger peak and the 50.8 mm projectile shows the most precipitous drop in K_{II}. After a normalized time slightly greater than 5, K_I begins to increase substantially in magnitude. In Fig. 2a the K_I values are the same for each projectile until $c_d t/l \sim 3$, which corresponds to the first reflection of the plane stress dilatational wave back to the crack tip. The values for the smaller projectile then begin to branch off and are much lower in magnitude. The 152.4 mm projectile values follow the rigid projectile until a normalized time of about 10. Then the larger projectile values increase with a more gradual slope than the other two. The values for all three seem to converge at later times.

The difference in the 50.8 and 152.4 mm deformable projectile stress intensity factor values is a consequence of an earlier loss of contact between projectile and specimen for the former case. Examination of the horizontal displacements for the nodes at the end of the projectile and the nodes in the impact area of the plate reveals that each node loses contact within 20–30 μs after impact ($c_d t/l \approx 4$–6.5) and complete separation can be seen at approximately 32 μs ($c_d t/l \approx 7$). It was thought the larger projectile should approximate a rigid projectile because reflections from the projectile's free end do not return to the plate–projectile interface until after contact is lost. However, this is not true because of the complex two-dimensional nature of the wave propagation in the specimen. The specimen loses contact with the projectile even for rigid projectiles (projectiles of infinite length). This loss of contact severely limits the duration of the K_{II} loading pulse at the notch tip, and consequently limits the possibility of initiating a shear localization there.

Examination of an infinite plate by Mason and Roessig [26] in a numerical extension of the solution of Lee and Freund [20] to long times has shown that K_I is linearly decreasing in time and K_{II} is increasing logarithmically in time for that geometry. Contact between the projectile and plate is not lost. Nor surprisingly, comparison of this result to finite specimens of various shape and size makes it clear that a larger specimen is advantageous because it will demonstrate a longer duration of monotonically increasing K_{II} loading at the notch tip. The monotonically increasing K_{II} is desirable because it can lead to larger plastic deformation and subsequent shear band initiation; however, the K_{II} loading can also lead to tensile failure at an angle of approximately 70°, as reported by Kalthoff [5], and shown schematically in Fig. 1a.

4.2. Effects of ageing condition on shear localization initiation

The three materials age-hardened at times of 0.5, 4 and 128 h each were first tested in tension at a strain rate of $10^{-3}\,s^{-1}$. The results are summarized in Table I, where the ultimate tensile strength, the strain hardening coefficient and the strain to failure are listed. Most

TABLE I Tensile properties of materials tested

Material	Tensile strength (GPa)	n	ε_f
Under-aged	1.86	0.0025	0.12
Peak-aged	2.10	0.0025	0.12
Over-aged	1.94	0.014	0.11

TABLE II Experimental results for under-aged 300 maraging steel specimens

Shot No.	Projectile length (mm)	Mixed mode crack angle (θ)	Velocity ($m\,s^{-1}$)	Failure mode
1	50.8	35	39.7	4 mm Mode II → Mode I
2	50.8	28	38.2	4 mm Mode II → Mode I
3	50.8	53	33.4	4 mm Mode II → Mode I
4	50.8	0	19.1	Small Mode I crack
9	50.8	26	33.0	Mode II → Mode I
5	152.4	0	10.0	None
6	152.4	62	20.6	Mode I
7	152.4		33.1	Full shear
8	152.4	0	10.2	None
10	158.8	0	32.8	Mode I
11	158.8	0	33.5	Mode I
12	158.8	0	42.7	Full shear

TABLE III Experimental results for peak-aged 300 maraging steel specimens

Shot No.	Projectile length (mm)	Mixed mode crack angle (θ)	Velocity ($m\,s^{-1}$)	Failure mode
5	50.8	29	38.5	19 mm Mode II crack
6	50.8	0	20.3	None
7	50.8	30	28.2	Small crack, possibly shear
9	50.8	0	34.1	Full shear
1	152.4	39	21.0	13 mm Mode I crack
2	152.4	0	21.0	None
3	152.4	15	21.0	13 mm Mode I crack
4	152.4	40	27.0	19 mm Mode I crack
8	152.4	0	33.7	Full shear

TABLE IV Experimental results for over-aged 300 maraging steel specimens

Shot No.	Projectile length (mm)	Mixed mode crack angle (θ)	Velocity ($m\,s^{-1}$)	Failure mode
1	50.8	0	33.0	1 mm Shear crack
2	50.8	0	48.1	2 mm Mode II crack
3	50.8	30	50.2	4 mm Mode II → Mode I
4	152.4	30	33.0	1 mm Shear crack

noticeable in the tension tests was the lack of homogeneous plastic deformation in these materials; necking occurred almost immediately upon yielding, indicating a very low work hardening rate and yield strength was nominally the same as the tensile strength. Using a simple criterion for necking [27] one can estimate the strain hardening exponent (n for a power law material, $\sigma = A\varepsilon^n$, where σ is stress, A is a constant and ε is strain) for both the under-aged and over-aged materials to be 0.0025. With such a low strain hardening rate the materials are very susceptible to shear localization indeed, as indicated by the criterion of Zener and Holoman in Equation 2. Since it was shown by Zhou *et al.* [15] that the peak-aged material is more susceptible to shear localization failure than a titanium alloy and given that titanium alloys have, in the past, been thought of as some of the most shear localization susceptible engineering materials available, it is likely that the low strain hardening rate in these materials makes them perhaps the most shear localization susceptible materials available. This characteristic has serious implications in the use of the testing geometry in Fig. 1 for testing of other, less shear localization susceptible, materials. It may be very difficult, if not impossible, to induce shear localization failure in other materials using this geometry as it is. Both under-aged and peak-aged materials have slightly different strengths, a fact that will have effects in the results to follow. The over-aged material, as shown in Table I has a higher strain-hardening exponent, 0.014, than either the under-aged or the peak-aged but its strength is roughly the same as the under-aged material. Based on the argument of Rogers [14], this fact would lead one to expect the over-aged material to be the most resistant to shear localization of all the materials.

Tables II–IV show the results of shear localization initiation tests conducted on specimens from the three age groups. The distinction between mode I and mode II failure was made by examining the fracture surface and/or path of crack propagation. A tensile (mode I) failure produces a crack which propagates at an inclined angle to the notch (at most 70°), and the fracture surface is rough with shear lips at the edges. High

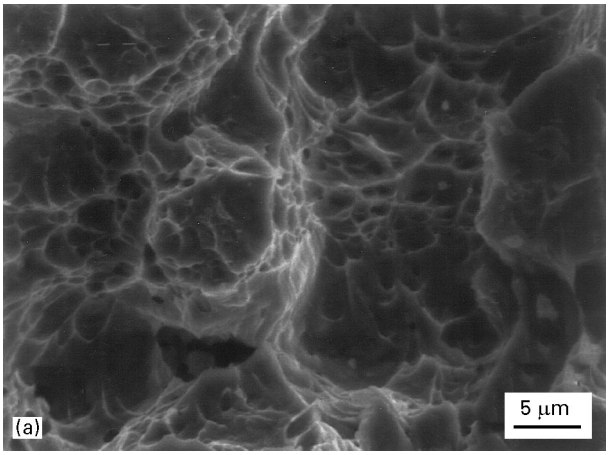

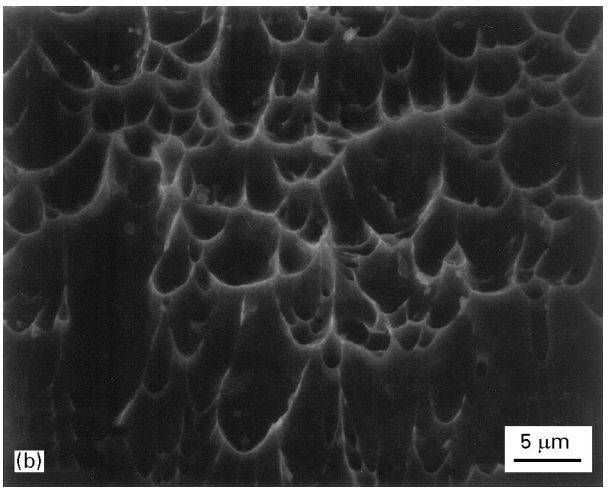

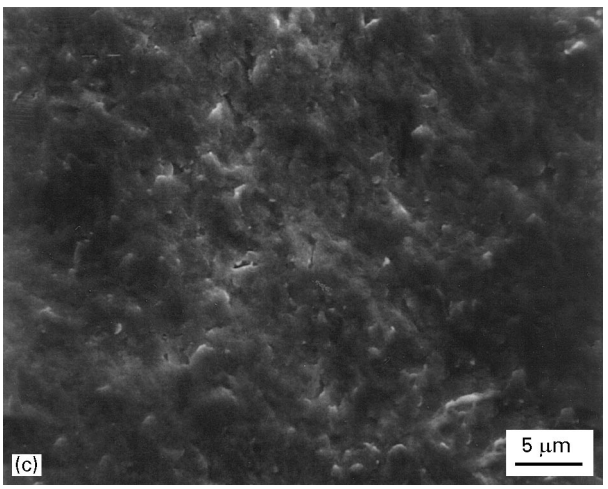

Figure 3 Micrographs of the fracture surfaces generated in the test shown in Fig. 5. (a) Fracture surface during crack opening dominated failure. (b) and (c) Fracture surface of shear dominated failure.

magnification examination of the fracture surfaces in a scanning electron microscope (SEM) reveals a ductile cup-and-cone failure mode, as shown in Fig. 3a. The damage surface for shear (mode II) failure looks very different. The cracks tend to propagate directly in front of the notch or at a small negative angle, and the fracture surface is relatively smooth with a shiny appearance to the eye. Examination of this surface in the SEM reveals shear voids, as shown in Fig. 3b, or very flat surfaces, as shown in Fig. 3c. There is no indication of any significant shear lips in the shear failure mode.

The critical velocity, V_{cr}, for which shear bands began to form for each ageing condition and projectile length is approximately $33\,m\,s^{-1}$. For under-aged specimens, the critical velocity was about $33\,m\,s^{-1}$ for both the 50.8 and 152.4 mm projectiles. When the smaller projectile was used at lower velocities (< 30 ms), small tensile cracks measuring less than 1 mm were observed. At higher velocities, like those used for shots 1–3 and 9, a small crack, up to about 4 mm, propagated directly in front of the notch and then continued to grow at an inclined angle, anywhere from 26 to 53°. This reported angle was a determined by the shear lips and, consequently, varies significantly from test to test. Examination of the fracture surfaces reveals that the initial growth is shear dominated and the latter growth is dominated by tensile crack opening. This change in crack propagation from mode II to mixed mode was consistently seen for this ageing treatment. It is interesting to note that for the higher impact velocities, like those used with shots 1 and 2, the extent of mode II damage was greater and the mixed mode crack propagation occurred at smaller angles. Using the 152.4 mm projectile at low velocities (about $10\,m\,s^{-1}$) produced no noticeable failure. A moderate impact velocity resulted in tensile failure on shot 6.

At higher impact velocities on the under-aged material the longer projectile resulted in full shear failure. This is quite possibly due to the longer duration of initial K_{II} loading from the longer projectile. It is known that the shear bands in this material accelerate after initiation [15]. If the acceleration to high velocity in the under-aged material is not completed before the arrival of reflected waves, it will likely arrest. The acceleration is probably retarded by the shorter K_{II} pulse in tests with the 50 mm projectile so that reflected loading can result in shear band arrest. When the longer projectile is used the shear band may accelerate more rapidly because of the higher average K_{II} resulting in full shear. Both results, full shear for the long projectile and arrested shear for the shorter projectile, are highly repeatable, and, at this point, the preceding explanation is offered tentatively.

The critical velocity for the peak-aged specimens is about $34\,m\,s^{-1}$ for both the 50.8 and 152.4 mm projectiles. The small projectile produced no damage for moderate velocities. A hit, at a velocity of $28.2\,m\,s^{-1}$, resulted in only a small crack, length less than 1 mm, for shot 7. However, full shear was observed with a velocity of $34\,m\,s^{-1}$. The highest velocity attempted with the 50.8 mm projectile resulted in nearly full shear, a 19 mm shear failure propagated directly ahead of the notch (shot 5). Using the 152.4 mm projectile and a moderate impact velocity ($21\,m\,s^{-1}$), either no damage occurred or a 13 mm tensile crack appeared. Shot 4 produced a 19 mm crack which, upon breaking the specimen apart for examination, was observed to be a tensile fracture. Full shear was obtained with the larger projectile and an impact velocity of $33.7\,m\,s^{-1}$.

The critical velocity values for the over-aged specimens are about $35\,m\,s^{-1}$ for the 50.8 mm projectile

and $33\,m\,s^{-1}$ (or slightly higher) for the 152.4 mm projectile. Only very small shear cracks were observed for impact velocities around $33\,m\,s^{-1}$. It was necessary to use high velocities for all the tests conducted for this ageing treatment. Increasing the velocity to $48\,m\,s^{-1}$ gave only a small mode II crack (4 mm). The largest impact velocity applied ($50.2\,m\,s^{-1}$) resulted in a transition from mode II to mixed mode. Examination of the fracture surface revealed shear localization extending for approximately 6 mm and tensile failure taking over the rest of the fracture. One test with the 152.4 mm projectile was conducted at $33\,m\,s^{-1}$. A small shear localization (< 1 mm) along with a small extent of tensile failure was observed. Concerns over safety prevented further tests at higher velocity with the massive 152.4 mm projectile. It is difficult to state the critical velocity for the 152.4 mm projectile, but it is interesting to note that full shear or complete fracture was never attained for this ageing condition.

The critical velocity did not depend on the ageing condition of the specimens or the length of the projectile. All values were in the 33–35 $m\,s^{-1}$ range, similar to that reported by Kalthoff [5, 6]. Zhou *et al.* [15] reported localization at lower velocities for the peak-aged material, but their notch radius was slightly smaller. The large size of their specimen and the type of projectile used could have had an effect, as it did in the under-aged material reported here. It is not surprising that the projectile length had no effect if initiation occurred before $c_d t/l = 3$ as reported by Mason *et al.* [7] and Zhou *et al.* [15]. At these values of early times, the stress intensity factor history is relatively independent of the projectile length. The insensitivity to ageing condition seems surprising. Based on the criterion of Zener and Holoman in Equation 2, one might expect the high strength materials, like the peak-aged material, to localize more easily. Surprisingly, that is not the case. It is possible that the dominant factor is the specimen size. As seen in Fig. 2, the stress intensity history for K_{II} at short times, $c_d t/l \leqslant 10$, in this geometry is roughly approximated by a half sine wave with a period given by four times the full width of the specimen, $c_d t/l = 8$. This determines the length of the "shear pulse" seen at the notch tip. Shear localization not only requires that the instability condition be satisfied, it also requires time to input plastic work to form and develop into a shear band followed by a shear crack. Possibly, given enough time the shear band could form at lower velocity; it would be necessary to increase the specimen width to check this presumption. In that case the ageing condition might have a greater effect.

Transition from mode II to mixed-mode crack propagation was prevalent in the under-aged condition, and to a lesser extent in the over-aged specimens. In the under-aged case, where more experiments were performed, the projectile length had an effect. A failure mode change was only observed with the shorter projectile. No mode change behaviour was observed in the peak-aged material, possibly because it has a higher propensity to shear localize than the other materials. It exhibited full shear failure more frequently than the other two materials.

The over-aged material showed little shear localization growth or final length even though it is roughly the same strength as the under-aged material. This is assumed to be a result of the higher strain hardening exponent in this material. As the hardening rate increases, the likelihood of thermal softening being large enough to cause localization decreases. The over-aged material, as a consequence, required higher impact velocities to generate shear bands of length equal to those in the under-aged material.

4.3. Effects of ageing condition on shear localization propagation

Having examined the effects of ageing condition on the shear localization critical impact velocity, the propagation of the shear bands in under-aged and peak-aged materials was examined. These two materials were chosen because they demonstrate two types of behaviour: full shear and shear arrest followed by tensile failure. The results of impacting two materials at nominally $40\,m\,s^{-1}$ with the 50.8 mm projectile are reported. For the first case, under-aged 300 maraging material, the resulting photographs of the material failure are shown in Fig. 4. At approximately 6 μs after impact, normalized time of 1.3, a shear failure began propagating directly ahead of the notch. Examination of the fracture surfaces after the test indicates that this is indeed a shear failure. This failure continues for approximately 14.5 μs and arrests at a total normalized time of 4.4 when the upward slope in K_{II} stops, as seen in Fig. 2. During that growth period the notch is closing because of lateral expansion – this is to be expected due to the negative K_I, as shown in the analysis of Lee and Freund [20] and the finite element model here – and the notch faces come into contact at approximately the same time that the shear crack stops growing. It is not clear whether the shear crack arrests because of the peak in K_{II} or the contact of the faces, or both. Contact is held for about 27 μs. After this the notch begins to open, after a total normalized time of 10.2 corresponding to a minimum K_I in Fig. 2, until a total normalized time of 16.4, 29 μs later, when K_I becomes positive and a crack appears growing at an angle upward from the shear crack. The numerical solution presented above is no longer valid at this time because the shear band is of significant length, and the crack opens, effectively changing the geometry of the specimen. This new crack is tensile and growing under mixed-mode, shear and tensile, loading. The transition corresponds to the change in K_I from compressive to tensile. The subsequent arrest of this secondary crack is not recorded. Clearly, this failure is a two-step process where each failure mode is distinct from the other. The arrest of the shear crack, well before the appearance of the tensile crack, appears to be caused by either the closing of the notch faces and the loss of a monotonically increasing K_{II} loading or both.

In the second case a peak-aged 300 maraging material was tested and significantly different results were

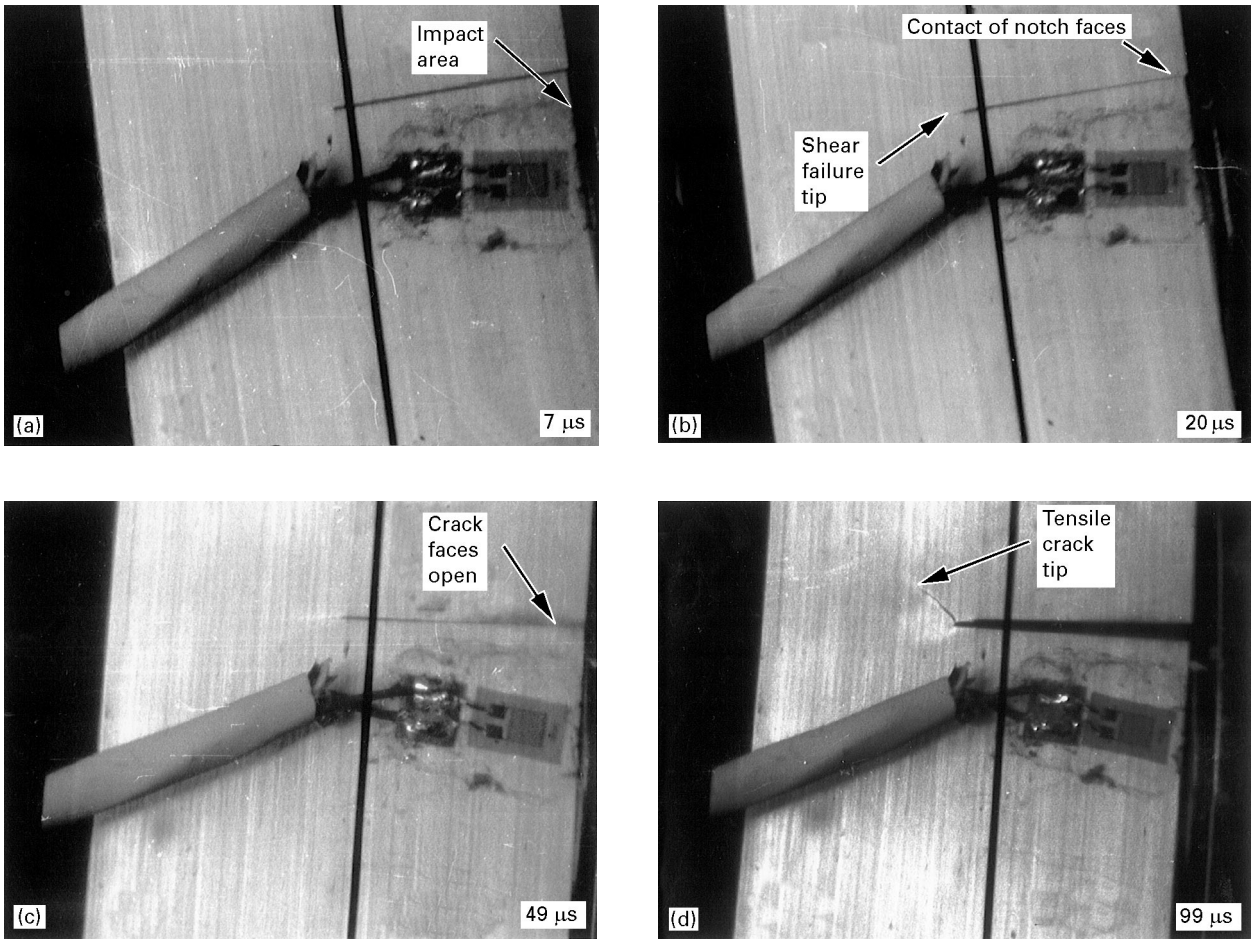

Figure 4 The dynamic fracture sequence of under-aged 300 maraging steel. The vertical black stripe is light removed from the photographs by the Cordin 330 camera for streak photography, if needed.

observed. The photographs of the material failure, taken at slightly higher magnification than in the previous case, are shown in Fig. 5. As with the under-aged material, at approximately 6 μs after impact, a normalized time of 1.3, a shear failure began propagating directly ahead of the notch. However, this failure propagates more rapidly than in the under-aged material; in the peak-aged material the shear failure propagates at approximately 1000 m s^{-1}, a typical speed for dynamic fracture in steel, whereas in the under-aged material the propagation rate was much slower, 300 m s^{-1}. The crack length is plotted as a function of time for the two cases in Fig. 6. Because of the uncertainty in the crack length measurements, not shown, only the average velocity is reported. Approximately 25 μs after initiation, a normalized time of 6.6, the shear failure has traversed the 25 mm uncracked section of peak-aged specimen in Fig. 5 and fully failed the specimen. The unloading wave from multiple reflections cannot catch the shear band tip before complete failure, therefore there is no arrest of the shear band. Failure is complete before a significant drop in K_{II} can occur, although K_{II} has ceased to increase, and contact of the notch faces can occur. Again, during the shear failure the notch is closing due to lateral expansion, but in this case it has no effect upon propagation of the shear failure. But, as in the under-aged test, evidence of the notch opening is seen after a normalized time of 10.2 when the maximum negative K_I is achieved. After shear failure, the opening mode serves to propel the two separated pieces away from each other. It appears that the material failure and separation occurs in the shear mode since at later times the crack opens in approximately 4 μs, which corresponds to an exceedingly high crack speed of 6000 m s^{-1}, well beyond the theoretical maximum speed or any experimentally measured speed in steels [28]. The failure is a one-step process dominated by shear failure.

The difference in the propagation of the shear localization in the under-aged and peak-aged material when impacted at 40 m s^{-1} with a 50.8 mm projectile is a reflection of the differences in strength of the two materials; they have essentially the same hardening exponent and ductility. To the best of our knowledge, this is the first demonstration of the isolated effect of material strength on shear localization behavior. Because the difference in strength is small, less than 10%, it does not affect the initiation and the critical impact velocity for localization significantly, but it affects the propagation dramatically. The exact mechanics resulting in the difference in propagation are not easily discerned. But, one can surmise that in the stronger, peak-aged material the plastic zone size at the notch tip is smaller and the work rate is higher; therefore the heat rate is higher and the amount of energy spent on changes in inertia is lower (assuming adiabatic conditions for simplicity). Consequently, it is expected that

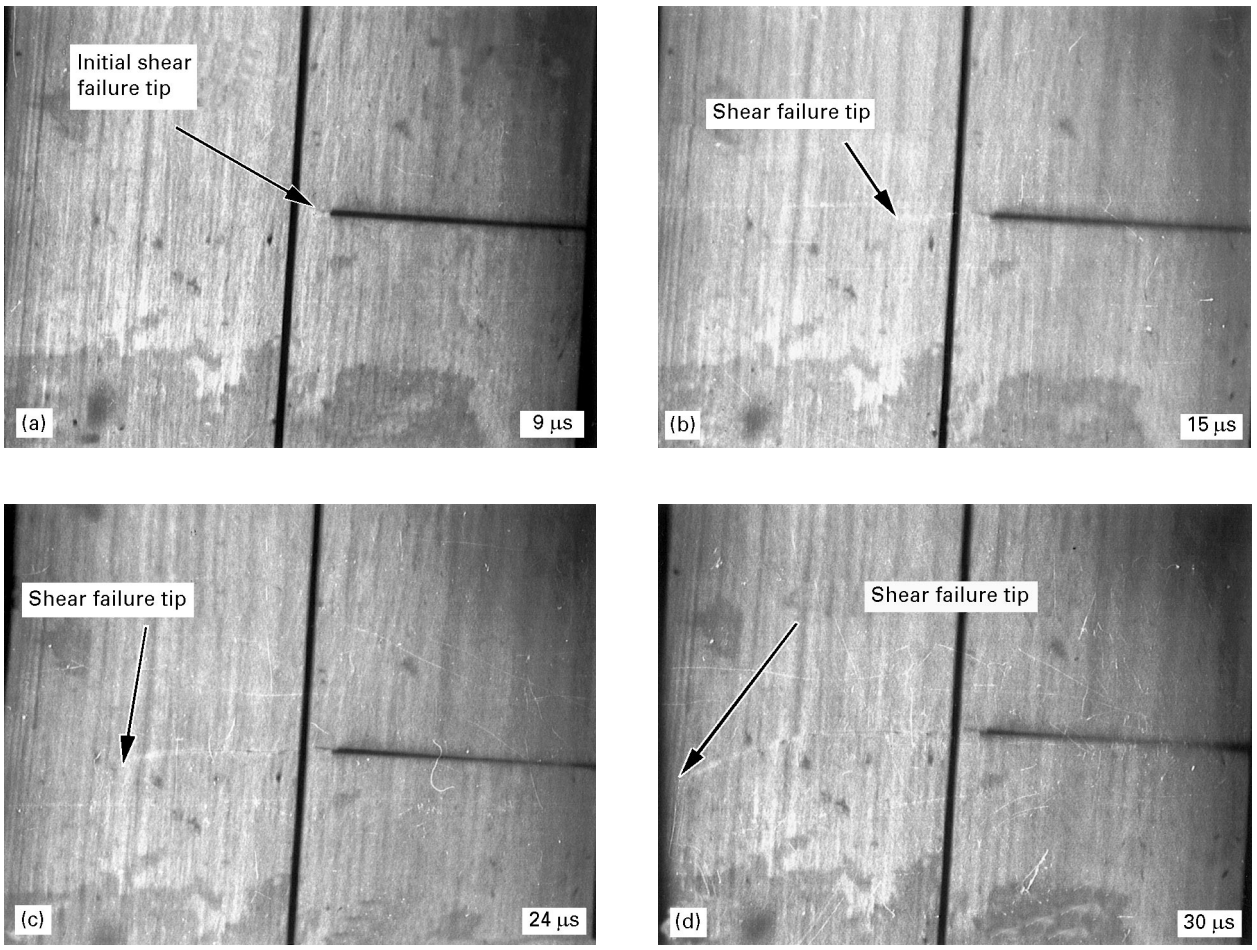

Figure 5 The dynamic fracture sequence of peak-aged 300 maraging steel.

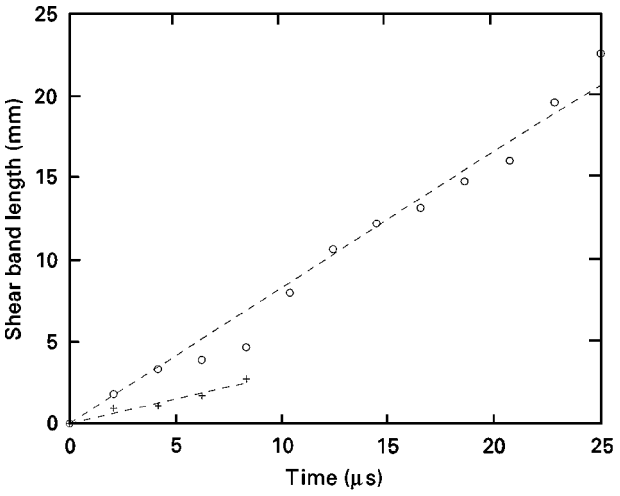

Figure 6 The length of the shear bands as a function of time after impact. Uncertainty in the length measurement prevents meaningful evaluation of shear band speed as a function of time. The average speed is taken from the linear fit shown. (○) peak-aged; (+) under-aged.

this material reaches a temperature and strain necessary for localization more rapidly and more efficiently than the lower-strength under-aged material. During propagation the plastic deformation ahead of the shear band must localize; because the plastic zone is initially smaller in the peak-aged material there is less inertial resistance to this process, and the shear band acceleration rate and final velocity may be larger. Any model of shear localization propagation should include this observed effect of strength.

5. Conclusions

Kalthoff impact tests were used to induce shear localization in edge-notched 300 maraging steel plates. The specimens were tested in the under-aged, peak-aged, and over-aged conditions and impacted with projectiles of two different lengths (50.8 and 152.4 mm). The initiation of shear localization did not seem heavily dependent on the ageing condition of the specimen or the length of the projectile. The critical impact velocity at which shear localization occurred was found to be independent of these experimental parameters; all of the critical velocities fell in the range of 33–35 $m\,s^{-1}$. These velocity values agree quite nicely with those found by Kalthoff for similar materials and notch radii in this range [5], but they do not agree with results of Zhou *et al.* [15], possibly because of differences in specimen size, notch radius and projectile length which determine the duration and intensity of shear loading at the notch tip.

Transition from mode II to mixed-mode crack propagation was consistently seen in the under-aged specimens and sometimes in the over-aged group. In the under-aged material failure mode transition behaviour did depend on the length of the projectile, as it only occurred in the under-aged material when the smaller projectile was used. This transition in failure

mode was not observable in the peak-aged group for these specimens because the shear band was able to traverse the entire specimen before unloading waves arrived to arrest it.

A simple elastodynamic, two-dimensional, finite element model of the steel plate and projectiles was created to assist in understanding the experimental results. The stress intensity factor history at a stationary notch tip in the experimental geometry was found for long times after impact. Assuming conditions of small scale yielding, this gives information about the deformation at the notch tip. While the elastic model becomes invalid as soon as crack or shear band propagation occurs, it does give some intuitive information about the observed change of crack propagation mode from shear dominated growth to crack opening dominated growth. Final shear band length is determined by a competition between the acceleration of the shear band and arrival of unloading waves at the notch tip either due to reflections from the specimen surfaces or loss of contact with the projectile. In the simulations, contact between the plate and projectile was lost within the first 32 μs, $c_d t/l \approx 7$, after impact. The calculated stress intensity factor history shows a mode II dominated crack tip stress field up until a normalized time of 10, where a mode I dominated crack tip field takes over. At later times, the K_{II} values were seen to increase again as the K_I values decreased. The model demonstrates that the Kalthoff geometry is best when the projectile is longer than the specimen is wide. Ideally, a semi-infinite specimen is desired so that monotonically increasing mode-II loading is generated. However, because that ideal cannot be achieved, the duration of shear loading in this geometry is limited by specimen size and, consequently, there are limits to the types of materials that can be failed by shear localization using this test geometry.

The shear band propagation was found to be very dependent upon the ageing condition. Under the same testing conditions, shear bands in the under-aged material propagated at velocities ($300\,m\,s^{-1}$) well below those of the peak-aged material ($1000\,m\,s^{-1}$). This is most likely to be caused by the slow acceleration of the shear band in the under-aged material after initiation, which is a reflection of the lower strength in the material. It is thought that the lower strength leads to a larger plastic zone at the notch tip which, in turn, requires more work for localization because of inertial resistance to deformation. As the propagation behaviour can be very sensitive to the ageing condition it is recommended that extreme care be taken in heat-treating 300 maraging steel samples for examination in this testing geometry.

Acknowledgements

J.J. Mason and K.M. Roessig would like to acknowledge the Air Force Office of Scientific Research and the Armament Directorate of Wright Laboratory at Eglin AFB for support of this work under the Summer Research Extension Program through grants RDL 96-0847 and RDL 96-0872, respectively. J.A. Zimmerman acknowledges the support of the University of Notre Dame.

References

1. A. MARCHAND and J. DUFFY, *J. Mech. Phys. Sol.* **36** (1988) 251.
2. J. H. GIOVANOLA, *Mech. Mater.* **7** (1988) 59.
3. *Idem.*, *ibid.* **7** (1988) 73.
4. A. K. ZUREK, *Metall. Mater. Trans. A* **25A** (1994) 2483.
5. J. F. KALTHOFF, in Proceedings of International Conference on Photomechanics and Speckle Metrology, SPIE, **814** (1987) 531.
6. J. F. KALTHOFF and S. WINKLER, in "Impact loading and dynamic behavior of materials", edited by C. Y. Chiem, H. D. Kunze and L. W. Meyer (Verlag, New York, 1987) p. 185.
7. J. J. MASON, A. J. ROSAKIS and G. RAVICHANDRAN, *J. Mech. Phys. Sol.* **42** (1994) 1679.
8. C. ZENER and J. H. HOLOMAN, *J. Appl. Phys.* **15** (1944) 22.
9. M. A. MEYERS, in "Dynamic behavior of materials" (John Wiley & Sons, Inc., New York, 1994) 459.
10. R. J. CLIFTON, J. DUFFY, K. A. HARTLEY and T. G. SHAWKI, *Scripta Metall.* **18** (1984) 443.
11. Y. BAI and B. DODD, in "Adiabatic shear localization, occurrence, theories and applications" (Pergamon Press, New York, 1992) p. 126.
12. R. C. BATRA and C. H. KIM, *Int. J. Plast.* **8** (1992) 425.
13. L. CHEN and R. C. BATRA, *J. Mech. Phys. Sol.* submitted.
14. H. C. ROGERS, *Ann. Rev. Mater. Sci.* **9** (1979) 283.
15. M. ZHOU, G. RAVICHANDRAN and A. J. ROSAKIS, *J. Mech. Phys. Sol.* **44** (1996) 1007.
16. *Idem.*, *ibid.* **44** (1996) 981.
17. D. E. GRADY, *ibid.* **40** (1992) 1197.
18. V. RAMACHANDRAN, X. J. ZHANG, R. W. ARMSTRONG, W. H. HOLT, W. MOCK, Jr. G. SOPER and C. S. COFFEY, in "Microstructure property relationships in titanium alloys", edited by Y. Kim and R. R. Boyer (The Minerals, Metals and Materials Society, Warrendale, PA, 1991) p. 111.
19. S. FLOREEN, in "American Society for Metals Handbook", Vol. 4 (ASM International, Metals Park, OH, 1981) p. 130.
20. Y. J. LEE and L. B. FREUND, *J. Appl. Mech.* **57** (1990) 104.
21. ABAQUS/Standard, Hibbitt, Karlsson and Sorenson, Inc., 1080 Main St, Pawtucket, RI, 02860-4847.
22. V. MURTI and S. VALLIAPPAN, *Eng. Fract. Mech.* **23** (1986) 585.
23. R. C. BATRA and N. V. NECITAILO, *Int. J. Plast.* **13** (1997) 241
24. J. J. MASON, J. LAMBROS and A. J. ROSAKIS, *J. Mech. Phys. Sol.* **40** (1992) 641.
25. J. A. ZIMMERMAN, MS thesis, University of Notre Dame, Notre Dame, IN 46556 (1995).
26. J. J. MASON and K. M. ROESSIG, in Proceedings of the 22nd International Congress on High-Speed Photography and Photonics, October 1996, (SPIE 1997) in press.
27. R. W. HERTZBERG, in "Deformation and fracture mechanics of engineering materials" (John Wiley and Sons, Inc., New York, 1996) p. 24.
28. L. B. FREUND, in "Dynamic fracture mechanics" (Cambridge University Press, New York, 1990).

Received 29 April
and accepted 24 September 1997